Journal of Computational and Applied Mathematics 329 (2018) 37–50

Contents lists available at ScienceDirect

Journal of Computational and Applied Mathematics

journal homepage: www.elsevier.com/locate/cam

Geometric approach to detecting volumetric changes in medical images

Alexander Naitsat [a], Shichao Cheng [b], Xiaofeng Qu [c], Xin Fan [b], Emil Saucan [a,*], Yehoshua Y. Zeevi [a]

[a] Electrical Engineering Department, Technion, Haifa, Israel
[b] School of Software, Dalian University of Technology, Dalian, China
[c] Dalian Medical University, Dalian, China

ARTICLE INFO

Article history:
Received 30 October 2016
Received in revised form 17 July 2017

MSC 2010:
68u15
30C65

Keywords:
Change detection
3D medical images
Quasiconformal mapping
Distortion measures

ABSTRACT

We present a new quantitative method for detecting changes in 3D medical images. The dissimilarity between shapes is quantified as a measure of the effort it takes to deform one 3D region into another. Our main tool is an assessment of conformal and isometric distortions of mappings between volumes. Unlike most existing techniques for shape comparison, our algorithm operates both on triangular and tetrahedral meshes, and therefore can be applied both for closed simply connected surfaces, as well as for volumetric domains homeomorphic to a ball, with geometrically complicated boundaries. Furthermore we extend our main geometric distortion measure to higher dimensions, in a manner that allows for the dealing with spatial data at the maximal, as well as at all the lower dimensions.

1. Introduction

Voxel-based morphometry (VBM) is one of the most popular methods for detecting brain differences between two or more groups of subjects [1]. This fully automated method makes it possible for researchers with various expertise to perform reproducible studies that identify neuropathological abnormalities in patients with various neurological syndromes, e.g., depression, autism, and epilepsy [2]. However, VBM lacks the robustness necessary for individual comparisons, due to the fact that its group-wise smoothing and registration smear subtle individual differences. Additionally, VBM can only provide voxel-wise comparisons, but reveals no geometric distortions.

Numerous surface-based techniques have been developed to investigate shape changes. These techniques include conformal mapping, see, e.g. [3] and surface matching, such as [4], among many others. Surface-based analysis offers accurate shape representation to detect subtle shape changes. Nevertheless, this type of approaches is insensitive to volumetric changes caused by gray matter atrophy widely discovered in physiological diseases [2].

The present paper is, divided, essentially, into two parts. In the first part we propose a new geometric approach, based on quantitative evaluation of deviations from the behavior of conformal and isometric mappings in Euclidean space, to the problem of detecting volumetric changes for individual comparisons in medical images. Our input data is assumed to be a set of volumetric domains, or a set of simply connected closed surfaces that enclose well defined interior volumes. In order to detect discrepancies between geometric structures, we consider the energy or effort required to deform one 3D domain into another. In the second part we propose an extension of the main geometric approach to higher dimensions that enables us

* Corresponding author.
E-mail address: semil@ee.technion.ac.il (E. Saucan).

http://dx.doi.org/10.1016/j.cam.2017.07.024
0377-0427/

to properly deal with spatial data, at all the intermediate dimensions. Finally, an Appendix summarizes higher dimensional versions of the main invariants employed in the first part of the paper, as well as listing a number of related invariants that appear in the Imaging and Graphics literature.

2. Mathematical background

In this section we introduce the main mathematical notions that reside behind the change detection method we propose in the present paper, mainly the notion of deformation of a domain in $\mathbb{R}^n$, as well as the notion of quasiconformal mapping. While we do this for a generic dimension n, we shall concentrate first on the case $n = 3$, and only later return to the higher dimensional one.

We formally define a *a deformation function* $f : D \to \mathbb{R}^n$ to be a local diffeomorphism of an open domain $D \subset \mathbb{R}^n$, i.e. for each point in $x \in D$ there exists a neighborhood of x where f is a smooth bijective mapping with a smooth inverse. Denote the set of the deformation functions by $\mathrm{Def}(\mathbb{R}^n)$. Moreover, since the Jacobian of a deformation is a full rank matrix, it has only positive singular values.

A homeomorphic deformation f of a domain $D \subset \mathbb{R}^n$ is called a *a conformal mapping* if for each point $x \in D$ it locally scales the space uniformly in every direction. This can be stated formally as

$$\|df_x(h_1)\| = \|df_x(h_2)\|, \tag{1}$$

where df_x denotes the Jacobian matrix of a function $f : D \to \mathbb{R}^n$, at a point x, and $h_1, h_2 \in \mathbb{R}^n$ are arbitrary unit vectors. Using this notation, we can bring also the next essential definitions for us: A conformal deformation $f(x)$ of a domain $D \subset \mathbb{R}^n$ is called *volume preserving* (or *equi-volume* deformation) if

$$\forall x \in D : |\det df_x| = 1. \tag{2}$$

A volume preserving conformal mapping is called an *isometry*.

While conformal mappings are abundant in 2D (in fact, they are, at least in the planar case, rather generic), volumetric domains can be mapped in general only *quasi-conformally* (see e.g., [5]), which means that the condition (1) is replaced by the uniform comparability of $\|df_x(h_1)\|$ and $\|df_x(h_2)\|$, for all unit vectors $h_1, h_2 \in \mathbb{R}$, with some constants depending on x. In this case we say that the mapping produce *conformal distortion* of the space. Applying the same terminology for isometries yields the concept of the *isometric distortion*.

We refer to conformal and isometric distortions as a *local metric distortions*. These represent local measures associated with a spatial deformation between given source and target regions. Using the Euclidean metric, we can express the volumetric distortions as simple functions of the singular value of deformation's Jacobian. The advantage of this method over other techniques that are used in volumetric modeling (e.g., discrete harmonic energy [6]) is that we can employ the same framework to deal with a wide range of spatial distortions and energies. For instance, the aspect-ratio distortion [7], several types of the rigid and affine energies considered in [8], the n-D conformality distortion [9], the angle and volume energies [10], all of which are expressed as functions of singular values. (See Appendix for the precise definitions of these notions.)

We summarize below the main mathematical definitions of volumetric distortions associated with f; for details and the theoretical background see [11] (as well as [12] and [13] for some first applications of these notions). While we restrict ourselves to the 3-dimensional case, these notions readily generalize to higher dimensions—see Section 7 as well as Appendix for the n-dimensional versions of these and of related invariants employed in the Imaging and Graphics literature.

The local conformal distortion of a quasiconformal map $f : D \subseteq \mathbb{R}^3 \to \mathbb{R}^3$, at point x, is measured by the so called *quasi-conformal* (qc) *dilatation* $K(x, f)$:

$$K(x, f) = \max\left\{ \frac{|\det (df_x)|}{\sigma_3 (df_x)^3}, \frac{\sigma_1(df_x)^3}{|\det (df_x)|} \right\}; \tag{3}$$

where $\sigma_1(df_x)$ and $\sigma_3(df_x)$ denote the maximal and minimal singular values of df_x, respectively. The minimal number K that satisfies condition (2) for all points x is called the *dilatation* of f and it is denoted by $K(f)$. (A somewhat more general definition, for all dimensions n, is given as condition (17) in Section 7 below. However, we do not bring here the most general form of the definition, since its technicality goes beyond the scope of this applicative papers—for details see, e.g. [11,14])

Alternatively, the conformal distortion can be estimated via the *linear dilatation*

$$H(f, x) = \frac{\sigma_1(df_x)}{\sigma_3(df_x)}. \tag{4}$$

(See also Appendix for the notation and terminology used in Imaging for this classical invariant.)

Similarly, we define local isometric distortion by

$$C(f, x) = \max\{\sigma_1(df_x), \sigma_3(df_x)^{-1}\}, \tag{5}$$

and the normalized version of the isometric distortion, also known as *k-bounded qi-dilatation* of f by

$$C_k(f, x) = \frac{C(f, x)}{k(\mathcal{S}, \mathcal{T})}, \tag{6}$$

where $k(\mathcal{S},\mathcal{T})$ measures relative sizes of source and target regions by the ratio of radii of their minimal enclosing spheres:

$$k(\mathcal{S},\mathcal{T}) = \max\left\{\frac{r(\mathcal{S})}{r(\mathcal{T})}, \frac{r(\mathcal{T})}{r(\mathcal{S})}\right\}. \tag{7}$$

To simplify numerical computations, we assume that, in our case, $k(\mathcal{S},\mathcal{T}) = 1$. However, to determine in the general case the fine geometrical features of the object via the *qi*-dilatation, one should use the *k*-bounded version.

Before proceeding further, let us note that the main distortion measures introduced above are related via the following double inequality (see also Appendix for its generalization to higher dimensions):

$$K(f,x) \le H^2(f,x) \le C(f,x)^4. \tag{8}$$

For the sake of completeness we also introduce the notion of *local volume distortion*. This quantity is closely related to volume preserving transformation, defined by

$$V(f,x) = \max\{|\det(df_x)|, |\det(df_x)^{-1}|\}. \tag{9}$$

Global changes in the geometric structure can be assessed by the average values of the scalar functions $K(f,\cdot)$ and $C(f,\cdot)$. In general, we denote the average value of a function $F : D \subset \mathbb{R}^3 \to \mathbb{R}$ by

$$\bar{F} = \frac{1}{\text{volume}(D)}\int_D F(\boldsymbol{x})d\boldsymbol{x}. \tag{10}$$

Following this notation, the discrepancy between $\mathcal{S}$ and $\mathcal{T}$ is represented as a point $(\bar{K}(f), \bar{C}(f))$ in the distortion plane. In particular, if $\bar{K}(f) = \bar{C}(f) = 1$ we achieve the maximal resemblance between geometric structures: In this case the target and the source regions are mutual images under a rigid transformation.

Recall that, by the classical Liouville Theorem (see, e.g., [15]), every conformal mapping of a domain in the Euclidean space $\mathbb{R}^n$, $n \ge 3$ is a restriction of a Möbius transformation (i.e. of a finite composition of inversions in sphere, reflections in hyperplanes and similarities). Therefore, preserving angles and lengths is impossible for non-trivial spatial transformations (that is, mappings that are not Möbius transformation), we employ the resulting volumetric distortions as measures of the effort necessary in order to deform one geometric structure into another. In particular, this approach is useful for detecting geometric changes between similar shapes mapped onto a common target domain.

Remark 1. It is hard to avoid asking oneself the following natural question: Why should we prefer such a somewhat piecemeal approach, instead of making appeal to more powerful, systematic methods, such as *Beltrami coefficients* and *Teichmüllller maps*? Indeed, these approaches have been already successfully applied to similar problems [16–18]. Unfortunately, while, as already mentioned above, there exists an abundance of quasi-conformal mappings in dimension $n = 2$, *Mostow's rigidity theorem* (see, e.g. [19]) implies that the Teichmüllller is trivial in dimension $n > 3$, thus so are the associated Beltrami coefficients. Therefore, there is no possibility of extending these methods to the case of volumetric (and higher dimensional) data. However, not everything is lost: Contrary to the common philosophy there exists a *local Teichmuller space*. It quantifies, one might say, the existence of a *local quasi-conformal stability*: Mappings that are sufficiently close to identity are obtained via quasi-conformal deformations. (The technical definitions and proofs of the simple ideas above are quite laborious—for more details, see [20] and the bibliography therein.)

3. Volumetric deformations

A variety of techniques for morphing of polygonal meshes are used in computer graphics for registration and similarity assessment. However, there is no single robust algorithm to deform arbitrary surfaces one into another, and existing methods are all subjected to different local and global constraints, such as smoothness, convexity, various topological obstructions, etc. The similar problem of deforming volumetric domains is even more complicated and raises serious theoretical and technical challenges. Therefore, in order to deal with this extended problem, a number of conventions and simplifications are needed.

One first such assumption is that models are centered at the origin. In order to solve this issue with accessible tools, we consider some intermediate canonical regions, such as a ball, solid cylinder or a cube. We refer to embedding of a volumetric domain onto a canonical region as to *a canonical parametrization*. In particular, we are interested in canonical parametrization into a ball, described in [12] (see also [5]). This parametrization technique constitutes, essentially a stretching of lines segments connecting the origin with the boundary. It can be expressed in spherical coordinates as

$$(r,\varphi,\theta) \mapsto \left(\frac{rR}{d(\varphi,\theta)}, \varphi, \theta\right), \tag{11}$$

where $d(\varphi,\theta)$ is a distance from the origin to the farthest point on the boundary, measured along the radial angle $\angle(\varphi,\theta)$, and R is a radius of the bounding sphere, estimated as a half of the longest diagonal of the bounding box.

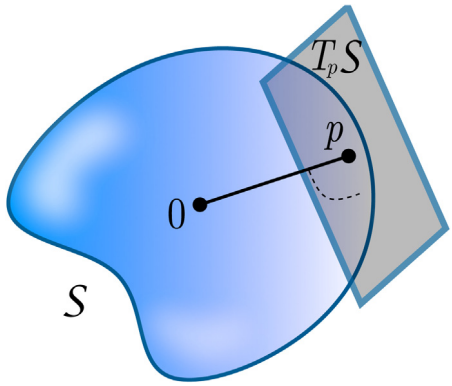

Fig. 1. Illustration of a star-shaped domain $\mathcal{S}$ that meets the geometric condition $\angle\left(\overline{0p}, T_p\mathcal{S}\right) \geq \alpha > 0$ for all $p \in \partial\mathcal{S}$.

If the source domain $S \subset \mathbb{R}^3$ is *star-shaped* at the origin, namely, if for any $p \in \mathcal{S}$: the line segment $\overline{0p}$ is also in $\mathcal{S}$, then the resulting mapping is onto. Moreover, (11) can be generalized to the following family of mapping onto a ball

$$f_a(r, \varphi, \theta) = \left(R\left(\frac{r}{d(\varphi, \theta)}\right)^a, \varphi, \theta\right), a > 0\,. \tag{12}$$

Caraman [5, p. 408] has shown that f_a is qc-conformal map of $\text{int}(\mathcal{S})$ for $a > 0$ (and thus it is a diffeomorphism) if the following geometric condition is fulfilled: $\mathcal{S}$ is star-shaped at the origin and for any $p \in \partial\mathcal{S}$ the angle between the line segment $\overline{0p}$ and tangent plane $T_p\mathcal{S}$ at p is larger than or equal to some constant $\alpha > 0$ (see Fig. 1).

Remark 2. Note that, while ostensibly the process we are describing evaluates the distortions of maps, rather than the geometry of the given spacial domain, by using mappings to a canonical domain (a ball), one actually estimates the quasi-conformal distance, so to say, between the given domain and the canonical one. Given that the mapping is both optimal and unique (which is not true for mappings between arbitrary domains) in case of the ball (see, e.g. [11]), this distortion, called *the coefficient of quasi-conformality* represents a measure of the quasi-conformal divergence of the given shape (domain) from the standard one, namely the ball. Let us also note that such an approach, namely representation on a standard "screen" (here, a ball) a common approach in Imaging Sciences. Moreover, as a mathematical idea, it can be traced back to one of the very definitions of conformality for planar mappings due to Ahlfors [21].

We should add that, both from a purely mathematically viewpoint, as well as for practical reasons, it is useful (and, indeed, natural) to consider, in certain cases, mappings to other standard domains, such as cones or cylinder (for instance, in the case of the hippocampus this last one could arguably be a natural choice). In such cases, the coefficient of quasi-conformality can be computed via one of the considered target domains, for which ready formulas are available (see [5]). Certainly, in our case, a departure from optimality of the mapping arises due to the need to pass via the canonical form via a somewhat heuristic procedure. (See also discussion in the sequel regarding the minimization of the distortion during the initial mapping.)

4. Discrete computations

A common way to represent volumetric data for numerical computations is to triangulate a continuous region D into tetrahedrons. This is a standard yet powerful technique applicable for various 3D structures. The resulting discrete object is called *a tetrahedral mesh*; formally it is defined as a 4-tuple (V, E, F, T), where V, E, F and T denote the vertex, edge, face and tetrahedon sets of the mesh, respectively.

Employing this approach to approximate a continuous deformation f yields a piecewise affine transformation f_s of the mesh interior, called a *simplicial map*. For a vertex $v \in V$ located at the position x, we set $f_s(v) = f(x)$. Next, we extent f_s to the interior of tetrahedra by 3D barycentric coordinates. According to [13] the gradient of a component $f_s^{(i)}$ inside a tetrahedral cell τ is

$$\nabla f_s^{(i)}(\tau) = -\frac{1}{3 \cdot \text{volume}(\tau)} \int_{j=1}^{4} \sum \boldsymbol{s_j} f_s^{(i)}(v_j)\,; \tag{13}$$

where $v_1, \ldots, v_4$ are vertices of τ, and $\boldsymbol{s_j}$ is the area of the face against v_j multiplied by its unit normal; see Fig. 4. All three components for $(i) = x, y, z$ are then combined to construct a constant Jacobian matrix inside τ, denoted by $df_s(\tau)$. The Jacobian matrix at a vertex $v \in V$ is approximated by the weighted average of $df_s(\tau)$ over the neighboring tetrahedrons. The corresponding numerical schemes were detailed in [12]. The last step in the estimation of the volumetric distortions $K(f, v)$ and $C(f, v)$ for each vertex, is to perform an SVD decomposition of the resulting Jacobian matrices, and substitute the

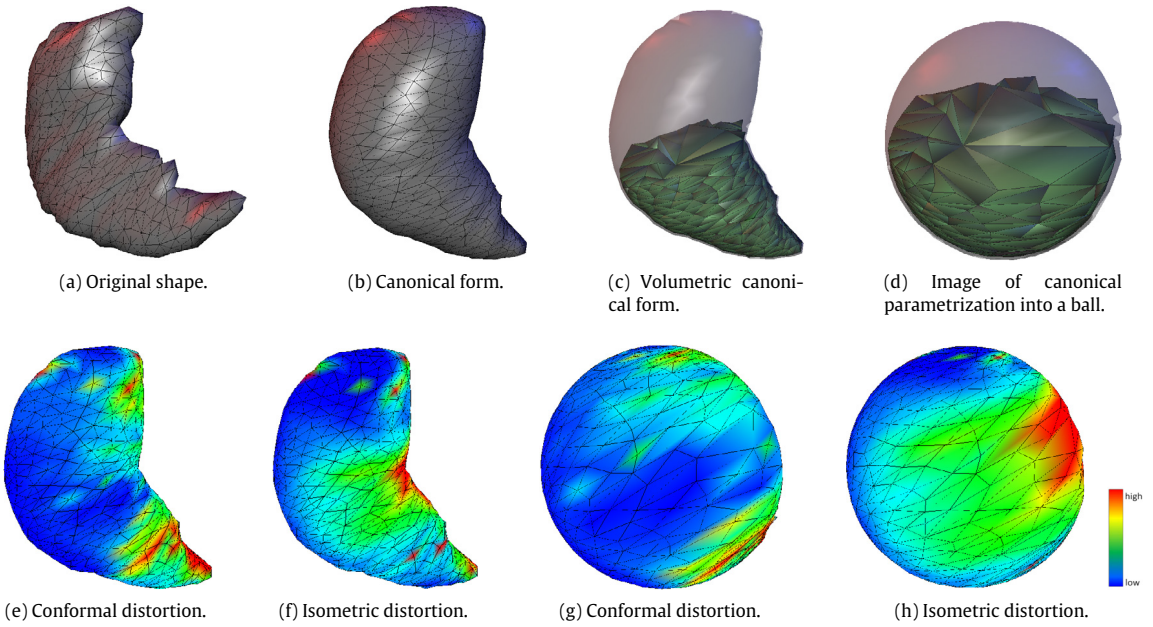

(a) Original shape. (b) Canonical form. (c) Volumetric canonical form. (d) Image of canonical parametrization into a ball.

(e) Conformal distortion. (f) Isometric distortion. (g) Conformal distortion. (h) Isometric distortion.

Fig. 2. Demonstration of Algorithm 1 applied on a surface shown in Fig. 3c. Figs. 2c and 2d illustrate volumetric models by showing cross sections of tetrahedral meshes. Figs. 2e and 2f depict, respectively, distribution of conformal and isometric distortions on the surface of the source domain; while Figs. 2g and 2h show the same distribution on the target surface.

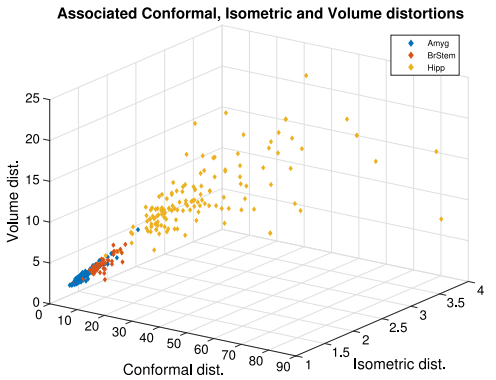

(a) 3D scatter plot.

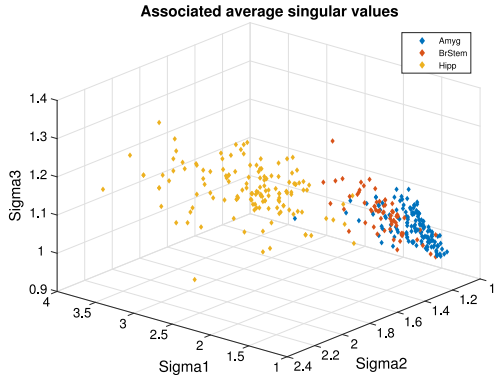

(b) 3D scatter plot.

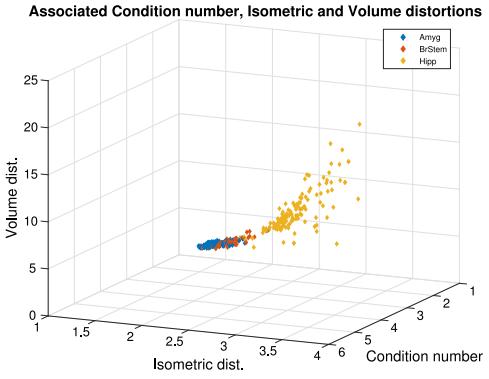

(c) 3D scatter plot.

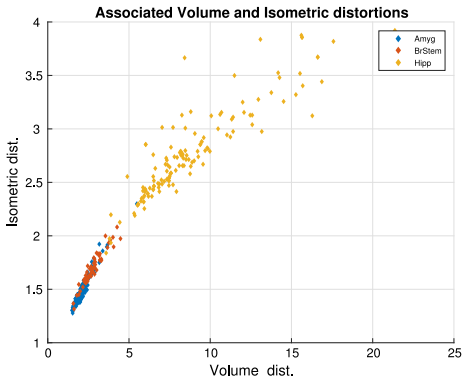

(d) 2D scatter plot.

Fig. 3. Scatter plots of various distortion measures associated with 3 types of brain segments: brain stem, amygdala and hippocampus.

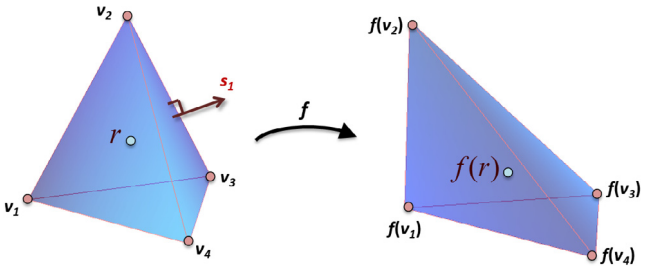

Fig. 4. Tetrahedron mapping and the corresponding constructions.

obtained singular values into Eqs. (3) and (5). According to [13] the formula for average distortions in a discrete case is the following approximation of Eq. (10):

$$\bar{F}(f) \approx \frac{1}{\text{volume}(D)} \sum_{v \in V} F(f, v) \cdot \text{volume}(\text{Cent}(v)), \tag{14}$$

where $F(f, v)$ is a local distortion of f at vertex v and $\text{Cent}(v)$ is a *barycentric cell* of v, obtained by connecting middle points of edges sharing v. Namely, for each cell τ in the vertex neighborhood we first construct a sub-tetrahedron by connecting v and middle points of edges sharing v. Then $\text{Cent}(v)$ is defined as the union of these sub-tetrahedrons over the neighboring tetrahedra of v.

In order to finalize our algorithm for real medical data, we should resolve the following issues:

1. Construction of an appropriate deformation between volumetric objects;
2. Computation of metric distortions in a discrete case;
3. Noise reduction to achieve an acceptable level of accuracy.

Algorithm 1: Metric distortions associated with a shape

Input:

Shape S represented by a polygonal mesh

1. Compute canonical form of S
2. Generate tetrahedral mesh $M = (V, E, F, T)$ contained in the canonical form
3. Construct mapping f_s of M to a ball by (11)

foreach $\tau \in T$ **do**

Estimate $df_s(\tau)$ according to (13)

foreach $v \in V$ **do**

Compute average Jacobian matrix at v

Compute $K(f_s, v)$ and $C(f_s, v)$

4. Estimate average distortions $\bar{K}(f_s)$ and $\bar{C}(f_s)$ according to (14)

Output:

Average metric distortions $\bar{K}$ and $\bar{C}$
associated with S

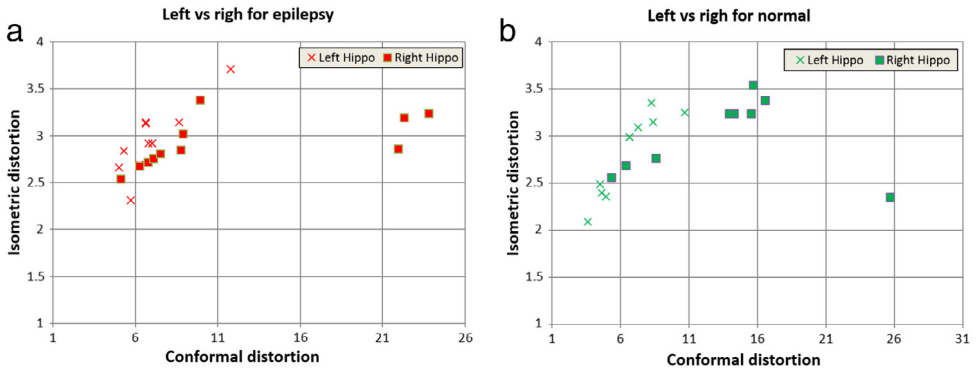

Fig. 5. Comparison between left and right hyppocampuses for healthy subjects and epileptic patients. Segments are represented on the distortion plane according to Algorithm 1.

5. Noise reduction

Like most computational techniques, our method of shape comparison may also be affected by the given level of noise. In [13] a typical noise was modeled as a composition of harmonic height functions on boundaries. In this case it has been shown that the resulting error in averaging the qc-dilation is a quadratic function of the noise amplitude and a linear function of the noise frequency. Similarly, the effect on the average isometric distortion appears to closely approximate a slowly increasing linear function of the noise parameters. This type of the noise is produced by the given limitations in the precision of scanning devices, hence the affected area is small relative to the dimensions of the whole region, and therefore the impact on the algorithm is usually insignificant.

However, some artifacts, like uncertainties in segmentation process, require additional preprocessing. Employing basic smoothing filters for artifacts removal may result in undesirable changes in geometric structures. Therefore, we took a different approach based on the so called *canonical representation* of surfaces.

The canonical form of a surface is a best approximation, w.r.t. geodesic distances, of the embedding of the surface into Euclidean space. This technique is often adopted in computer vision for complex surfaces, such as character models. Notably, employing this method for more isotropic structures that we have, provides an anti-aliasing filter for artifacts removal on the one hand, while on the other hand it preserves inner geometry of surfaces. Clearly, here the given surface, that is the boundary of the scanned volumetric object (e.g. hippocampus) is already embedded in $\mathbb{R}^3$.

Let S be a surface sampled at n points $\{p_1, \ldots, p_n\}$. First, using the fast marching algorithm [22] we compute a metric representation of S, which is an $n \times n$ matrix D, where D_{ij} is geodesic distance between p_i and p_j. Next, we construct the canonical mesh of S by classical multi-dimensional scaling [23]. The final outcome of the preprocessing stage is a *volumetric canonical form*, namely a tetrahedral mesh contained in the fitting canonical form of a boundary surface. In our case most canonical forms are star-shaped domains that satisfy the geometric condition illustrated in Fig. 1. Therefore, according to Section 3, these domains are mapped quasi-conformally onto a ball by (11). Moreover, since mapping (11) preserves θ and ϕ angles, the resultant distortions are independent of the domain orientation.

Algorithm 1 summarizes the main steps of our technique that includes: noise reduction, construction of volumetric deformations and estimation of the resulting spatial distortions. These steps are illustrated in Fig. 2 and in Fig. 8 for a hippocampus mesh and for meshes of other brain segments.

6. Experimental results

We collected 20 T1-weighted MRI images, 10 from epilepsy patients and 10 from age-matched controls. We used Freesurfer http://freesurfer.net/ to segment hippocampal regions of all these 20 brain images and obtained their meshes, where default parameters were applied for both segmentation and mesh generation. Subsequently, these hippocampal meshes were deformed onto a ball, and we applied our algorithm to estimate the conformal and isometric distortions of all left and right hippocampal regions.

We plotted the distortions in Fig. 5 by taking conformal distortions as x values and isometric distortions as y. Fig. 5a demonstrates the distortion distributions of epilepsy patients, where crosses denote the left side, while squares are the right side. As shown in Fig. 5a and b, the points from one side scatter along one common straight line, are indicating even volumetric deformations from a ball. Evidently, there exist three squared points deviating from the straight line of the right side of epilepsy patients. These points signify the abnormal volumetric deformations for epilepsy patients. Previous studies using group analysis based on VBM reported hippocampal volume abnormalities on the ipsilateral[1] side of seizure activity in

[1] I.e. appearing on or affecting the same side of the body.

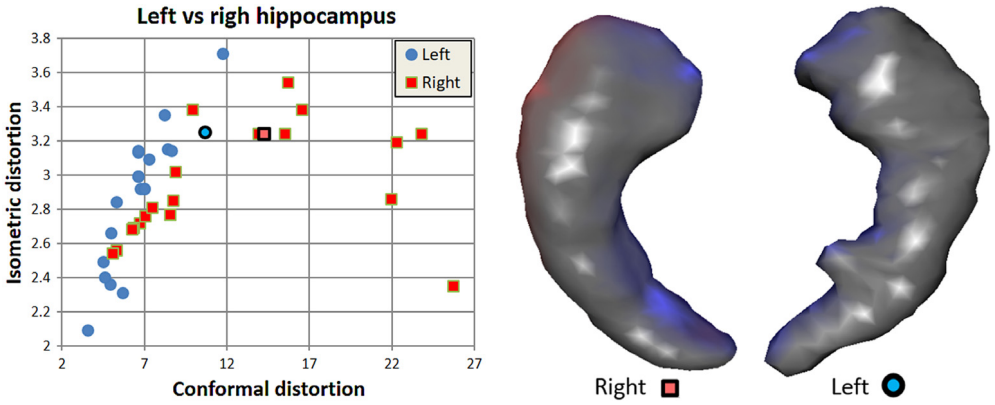

Fig. 6. The scatter plot depicts volumetric distortions of hippocampal regions. Two sides of the chosen individual hippocampus are highlighted in the plot and their shapes are shown on the right.

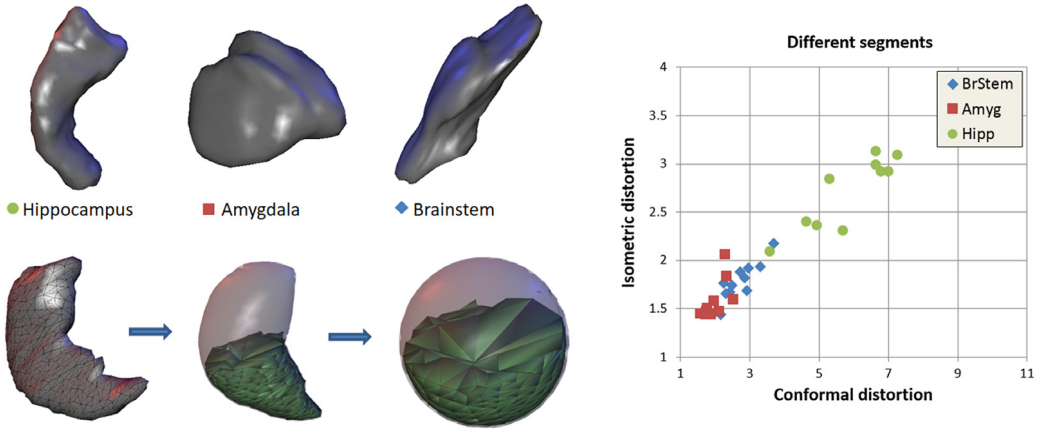

Fig. 7. Stages of the algorithms are shown on the top: original mesh, tetrahedral mesh of a canonical form and its image under deformation (11). Scatter plots show results of classification of brain segments: brain stem, amygdala and hippocampus.

patients [2,24–26]. It is worth noting that the hippocampal volume abnormalities or deficits were discovered by counting the voxels corresponding to the hippocampal regions. In contrast, we elucidate the volumetric distortions by two parameters. Moreover, we are able to perform individual volume comparisons between two sides as given in Fig. 6, where the volumetric deformations of both the left and right brain hemispheres of each subject are presented.

Fig. 3 shows the comparison of a few hundreds meshes of different brain segments. Each mesh is represented on a scatter plot by two or three distortion measures associated with the canonical mapping of the mesh into a ball. These results were obtained by applying, in each instance, Algorithm 1.

Compared with VBM, our approach has the merit of individual comparisons. On the other hand, this approach is likely to rely on the quality of segmentation and generated meshes. One outlier from the control group appears in Fig. 5b, showing great deviation. This deviation is attributed to the inaccurate segmentation for the right side of hippocampus for the subject. Additional human inspection and algorithm validation can be included in the future work.

7. A higher dimensional distortion estimate

The approach adopted above has, as a closer examination of our method shows, a number of drawbacks. Among these, locality is a one of them, while its dependence on smoothness (necessary on a Jacobian based approach) being another. Nevertheless, we have seen that how to overcome these limitations in practice, at least in a partial, yet satisfactory manner. (Smoothness, at least a.e., is also a theoretical consequence of the definition—see, e.g. [11].) However, its main detriment resides in the fact that it is not an intrinsically volumetric method: while it incorporates in the defining Formulas (3) and (4), it does this only directionally, without a measure (volume form) component. Additionally, Formula (9) represents a local condition, while the averaging Formula (10), while most natural, fails to capture the specific behavior of qc-mappings in all the intermediate dimensions.

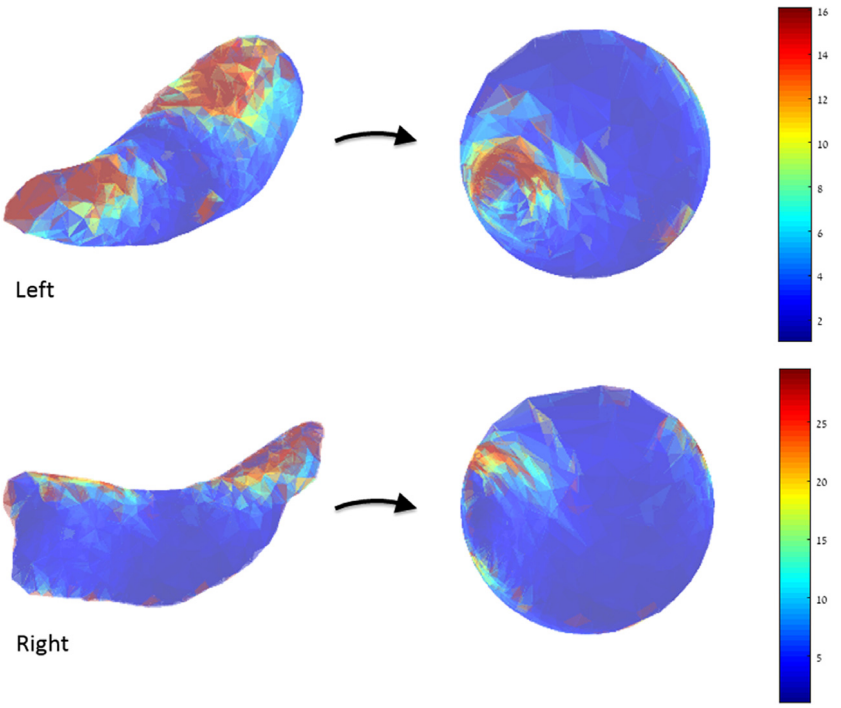

Fig. 8. Comparison of $K_{I,M}$ for the mapping of the left-side (above), respective right-side (below) of the hippocampus of a patient. Note the discrepancy between the two values—3520.5331 and 4433.5875, for the right-side, and left-side hemispheres, respectively, showing that even this weak upper bound for (7) represents a potentially efficient tool in discerning certain diseases via distortions in different dimensions. Here we considered tetrahedral meshes that were smoothened for the computation of the canonical form.

We suggest here an approach that both allows for the study of distortion in all dimensions and that, furthermore, is global and, moreover, does not necessitate any smoothness hypothesis. The proposed method is based on yet another approach to the definition of quasiconformality, distinct both from the *analytic definition* embodied in Formula (3), and the *metric definition*, that stands behind Formula (3) (see also Appendix). The third manner of defining the notion of quasiconformality, the so called *geometric definition* is based on the notion of *modulus* (*of a family of curves*):

Definition 1. Let Γ be a family of curves in $\mathbb{R}^n$ and let $\mathcal{F}(\Gamma)$ the family of admissible functions for Γ, namely the family of all Borel functions $\rho : \mathbb{R}^n \to [0, \infty]$ such that $\int_\gamma \rho\, ds \geq 1$, for every locally rectifiable curve $\gamma \in \Gamma$.

The *n-modulus* (which, for brevity reasons we shall refer below as simply the *modulus*) of Γ is defined as

$$M(\Gamma) = \inf_{\rho \in \mathcal{F}(\Gamma)} \int_{\mathbb{R}^n} \rho^n d\mathrm{Vol}\,. \tag{15}$$

It is important to note that the n-modulus represents a conformal invariant, thus rendering it as an important tool in the study of conformal and quasiconformal mappings, hence its relevance in our present study.

The modulus is related to the dilatation K of a quasiconformal mapping via the following double inequality: if f is a quasiconformal homeomorphism between two domains D_1 and D_2 in $\mathbb{R}^\times$ ($n \geq 2$), then

$$\frac{1}{K} M(\Gamma) \leq M(f(\Gamma)) \leq K M(\Gamma)\,; \tag{16}$$

for every family of paths Γ in D_1 (see, e.g. [27], Theorem 10.33), where K denotes, again, the dilatation of f.

Clearly, the double inequality (16) can be used to give an alternative (and equivalent) definition – the *geometric definition* of quasiconformality (and, in fact, only its right-hand side suffices) – see [11]. Moreover, while clearly the actual computation of the modulus represents a challenging problem, it turns out that for proving many of the essential properties of quasiconformal mappings, the modulus represents the most efficient and economical, so to say, tool.

In view of the power of Definition 1 above, it is only natural to look for its extension in higher dimensions. It turns out that, indeed, such a generalization is at hand. Evidently, instead of considering families of curves, one has to look at families of *k-dimensional hypersurfaces*, and, indeed, there exists a fitting generalization of the classical Formula (16). Before being able to formulate it we must, however, introduce some further notation:

The numbers

$$K_O(x,f)=\frac{\|df_x\|^n}{|\det df_x|}\,,\quad K_I(x,f)=\frac{|\det df_x|}{l(df_x)^n}\,; \tag{17}$$

are called K_O, K_I denote the *outer*, respective *inner* dilatations of f; where $\|df_x\|^n=\max\{df_x(h)\,|\,h\in\mathbb{R}^n,|h|=1\}$ (the operator norm of df_x with respect to the Euclidean norms considered, both in the domain and in the range $\mathbb{R}^n$); and $l(df_x)=\min\{\|df_x(h)\|\,|\,h\in\mathbb{R}^n,|h|=1\}$. Here we assume that df_x is not singular, a fact that holds a.e. x if f is quasiconformal.

We can now give the sought generalization of Formula (16):

$$\inf\int_\Omega\frac{\rho^n(x)}{K_O(x,f)}d\mathrm{Vol}\le M(f(\Gamma_k))\le\inf\int_\Omega K_I(x,f)\rho^n(x)d\mathrm{Vol}\,; \tag{18}$$

where each infimum is taken over all admissible functions for Γ_k, where (in a straightforward generalization of the classical, 1-dimensional case) $\rho:\mathbb{R}^n\to[0,\infty]$ is called *admissible* for Γ_k if $\int_{S_k}\rho dA_k\ge 1$, for any k-hypersurface $S_k\in\Gamma_k$; where dA_k represents the k-dimensional area element,

Remark 3. The outer and inner dilatations are closely interrelated via the following inequalities:

$$K_O(x,f)\le K_I^{n-1}(x,f),\quad\text{and}\quad K_I(x,f)\le K_O^{n-1}(x,f)\,. \tag{19}$$

Moreover, they are also related to the quasiconformal (or maximal) dilatation K, and in fact we have

$$K(x,f)=\max\{K_O(x,f),K_I(x,f)\},\,. \tag{20}$$

As already noted before, the actual computation of the modulus represents a quite difficult computational task, and we deffer it for later study. However, not everything is lost and the double inequality provides us with a simple way to compute the distortion induced by a map f in all dimensions $k=1,\dots,n-1$. Indeed, while precises estimates for $M(\Gamma_k)$, $M(f(\Gamma_k))$ are hard to achieve, it is intuitively clear that the ratio of these two quantities represents a measure of the distortion produced by f, in any dimension lower than n, and *independently* of the specific family of considered hypersurfaces. Therefore, it represents a measure of distortion of f itself. We are thus conducted to propose the following

Definition 2. Let f be a homeomorphism between two domains D_1 and D_2 in $\mathbb{R}^n$ ($n\ge 2$). We define the k-dimensional modulus distortion of f, or, in analogy with the classical, 1-dimensional case, simply the k-dilatation of f as being

$$M_k(f)=\sup\frac{M(f(\Gamma_k))}{M(\Gamma_k)}\,, \tag{21}$$

where the supremum is taken over all the families of k-hypersurfaces in D_1.

Clearly, $M_k(f)$, is bounded from above, as Formula (21) shows. However, the lower bound is also important, showing that there exists a minimal distortion as well, in any dimension, thus proving that one cannot try to achieve or even approach isometry/conformality in any dimension smaller than the maximal one, not just for the 1-dimensional (metric) case.

Before trying to find computable bounds for $M_k(f)$, at least in some special cases, let us first show the practical relevance of the notion just introduced. Since in medical imaging curves distortion is only one relevant task (e.g. for good "on screen" estimates for diagnosis and surgery planning), we concentrate on the surfaces case ($k=2$). Surfaces appear in medical imaging as membranes - the diaphragm, the meninges and the atrioventricular and interventricular septa being exemplary instances. They also arise, of course, as the exterior (observable) surfaces of internal organs (e.g. the prostate) or tumors. In some instances, the organ itself, or at least its interior face is, essentially, a surface, such as in the case of stomach or of the colon. While in theory one can compute $M_k(f)$ for any family of surfaces, in practice one usually deals with families of surfaces composed of a single element (as in most of the examples) above. However, it is important to notice that one is not restricted to simple cases, nor just smooth ones, but can rather also study branched surfaces, by viewing them as representing a family of intersecting surfaces. We see, therefore, that one has a wide spectrum of possible medical usages of the 2-*dilatation*. The main apparent drawback of the suggested approach resides in the fact that it only holds in dimension strictly smaller than n, thus, for Medical Imaging, it does not allow for the measurement of a "true" volumetric dilatation. However, in practice, medical images, such as CT ones, are obtained during temporal processes, thus rendering an extra, time dimension, giving the observed data a simple (product) 4 dimensional structure embeddable in $\mathbf{R}^4$. Thus one can view just on instance ("frame" of the "movie") as 3-hypersurface in $\mathbf{R}^4$ and compute M_3, without needing to visualize the 4-dimensional structure. Another approach would be to add a small, predetermined quantity of (e.g. Gaussian) noise to obtain a similar 4-dimensional product structure that allows the computation of M_3.

Having demonstrated the relevance and potential usefulness of our proposed method, we can now concentrate on its feasibility in practice. There are too aspects that we should address.

First, one has to agree that, clearly, M_k is problematic to compute from Formula (7) in the general case, at best. However, for the tetrahedral meshes that constitute the substrate, so to say, of our computations, one can easily calculate

$$K_{I,M}=\max\{K_I(x,f)\,|\,x\in D_1\}\ \text{ and }\ K_{O,m}=\min\{K_I(x,f)\,|\,x\in D_1\}\,, \tag{22}$$

thus obtaining coarse estimates for $M_k(f)$. (An illustration showing the potential in diagnosis of these invariants is presented in Fig. 7.)

The second aspect we should address is that of the smoothness of f. Indeed, while in many applications in Imaging, Graphics and CAGD functions are supposed to be smooth, there is a contrast between this assumption and the type of data one has to handle, i.e. at best polygonal/polyhedral meshes (and, in many cases, this only after highly nontrivial preprocessing). Therefore, one is entitled and, indeed, conduced to ask whether this hypothesis cannot be weakened substantially. It turns out that, at least for the case at hand, this is quite easy. We present here, succinctly and as simply as possible, the situation for meshes—for the full technical intricacies in the most general case we refer the reader to [27]. We begin by making the observation that mappings between (compact) polyhedral (and in particular, tetrahedral) meshes are not only *Lipschitz* but, in fact, *bi-Lipschitz* (i.e. f^{-1} is also Lipschitz). To this end we add the extremely mild and usually encountered in practice condition, that f produces no collapse both in a metric sense (i.e. no edge collapse), and in measure (e.g. for triangular meshes, no triangle collapse). In this case we shall say that f has *finite metric distortion* and denote this succinctly by $f \in$ FMD. It turns out (see [27] and the references therein) that if $f \in$ FMD automatically implies that it is differentiable a.e., which shows that we do not have, in fact, to prescribe a priori the smoothness of our maps.

If in addition f does not collapse areas for any hypersurface S_k, $k = 1, \ldots, n-1$, it is called of *finite area distortion* ($f \in$ FAD). Surprisingly enough, the condition that a bi-Lipschitz homeomorphism f has no metric collapse, suffices to ensure that $f \in$ FAD.

The importance of this result resides in the fact that, for FAD maps the desired analogue of right-side inequality in (16) holds, namely

$$M(f(\Gamma_k)) \leq \int_{D_1} K_I(x, f)\rho^n(x)d\mathrm{Vol}_1 . \tag{23}$$

Note that, in contrast with (18), there is no inf appearing here, and not just due to passing to finite meshes. (Indeed, a min does not appear either.)

Furthermore, a similar estimate exists for $M(\Gamma_k)$ as well, namely

$$M(\Gamma_k) \leq \int_{D_2} K_I(y, f^{-1})\rho^n(y)d\mathrm{Vol}_2 ; \tag{24}$$

where here $K_I(y, f^{-1})$ represents a succinct notation for $\sum_{\xi \in f^{-1}(y)} K_O(\xi, f)$.

Moreover, one can extend (16) to bi-Lipschitz mappings that are not homeomorphism, by imposing the following two conditions that, together, generalize the notion of quasiconformality:

(i) f is *open*, i.e. f maps open sets onto open sets;

and

(ii) f is *discrete*, i.e. the preimage under f of any point composed of isolated points.

Note that condition (ii) holds trivially for maps between the considered polyhedral meshes, since the preimage of any point consists of a finite number of points. Moreover, condition (i) is easy to interpret if we restrict ourselves to neighborhoods (of vertices): it simply states that the open star of any vertex cannot collapse under f.

We should note that allowing for condition (ii) to hold, permits us to consider maps that exhibit foldings and branchings (and that are, in fact, quasiconformal in the classical sense away from the branching set—see [27] and the bibliography therein).

It turns out that maps of the more general type introduced above, also satisfy a variation of (16). In fact, the left-hand inequality holds precisely in the same form like in the more classical context, while the right-side one holds for $K_I(x, f)$ being replaced by $K_I(y, f^{-1})$ (the notation being as above).

So we see that, while by Formula (19), the inner and outer dilatations are interrelated, and with the maximal dilatation K as well, they are quite necessary in measuring the higher-dimensional distortions (dilations). Moreover, in view of the results above, the pair (K_O, K_I) presents itself as a potentially very useful additional classifier for the shape recognition, matching and related tasks, especially in dimensions ≥ 3, and in particular for detecting volumetric changes in volumetric data.

8. Conclusions and future work

We have presented a new quantitative method for detecting changes in volumetric models with applications to medical imaging. Our approach is based on assessment of average conformal and isometric distortions associated with a deformation of 3D segment into a ball. Since our algorithm operates on tetrahedral meshes, it can be applied on both closed simply connected surfaces by generating interior tetrahedra, as well as in volumetric domains with more sophisticated boundaries.

Our future work is primarily aimed to improve the accuracy of the results. One main, computational approach under current research consists in employing additional distortion measures (see Appendix) and to minimize the impact a particular choice of the mapping has on the results.

Distortions produced by a mapping $f : \mathcal{S} \to \mathcal{T}$ are usually expressed via the Jacobian's singular values (cf. Appendix below), which in 3D are roots of a 6^{th}-degree characteristic polynomial of $dfdf^T$. Therefore, in general, it is hard to estimate

the effect each deformation has on conformal and isometric distortions. A more feasible approach is to consider an *optimal mapping* with respect to a chosen distortion measure $D(f, x)$ (e.g., $D(f, x) = K(x, f)$):

$$f_{\text{opt}} = \underset{f:\mathcal{S}\to\mathcal{T}}{\operatorname{argmin}} \int_{\mathcal{S}} D(f, x)\, dx. \tag{25}$$

Since f_{opt} depends entirely on the geometry of both source and target domains, we expect that employing optimal mappings can significantly improve the precision of Algorithm 1. We intend to obtain well approximated solutions of (25) in the discrete case using gradient descent in conjunction with variational methods.

Another natural further direction of study would be directed to obtain better estimates (and, indeed, trying to obtain as precise as possible computations) for the higher dimensional distortions introduced in Section 7, that is towards the development of numerical methods of estimation (and computation) of k-dimensional moduli (with special aspect being still placed on the classical case, that is the calculation of the modulus of curves).

We should finally note that, in view of Remark 1, not everything is lost as far as the extension to higher dimensions of Teichmuller space methods is concerned. True, as we have seen, there is seemingly no hope in making appeal to extensions of the classical Beltrami coefficients. However, while the theoretical apparatus and reasoning are quite involved, the said local deformations are geometric and quite intuitive, and furthermore, they algorithmic in nature. Thus, there exists the hope of replacing the analytic methods of distortion minimization by a geometric approach based on the application of a sequence of possible deformations, each reducing to a standard construct.

Acknowledgments

The research of Y. Y. Zeevi was supported by the OMEK consortium and by the Ollendorff Minerva Center for Vision and Image Sciences. Emil Saucan's research was partly supported by the National Natural Science Foundation of China Grant No. 61572105. He is also glad to acknowledge the support and warm hospitality of the Max Planck Institute for Mathematics in the Sciences, Leipzig, where a substantial part of this paper was written.

Appendix

We list below the formulas for n-dimensional versions of the main invariants considered in the first part of the paper, as well as a number of other distortion measures that were considered in the literature by various authors. We express all these measures as functions of the singular values of Jacobian $\sigma_i = \sigma_i(df_x)$, $i = 1, \ldots, n$.

We begin with the mathematical notions employed in the paper (for further details see [5,11]):

- *The quasiconformal dilatation*

$$K(x, f) = \max\left\{ \frac{\sigma_1 \cdots \sigma_{n-1}}{{\sigma_n}^{n-1}}, \frac{\sigma_1^{n-1}}{\sigma_1 \cdots \sigma_{n-1}} \right\}. \tag{26}$$

- *The linear dilatation*
  It is formally defined, in a manner extendible to quite general metric spaces, as

$$H(f, x) \triangleq \limsup_{r\to 0} \left(\frac{\max_{y\in\mathbb{S}(r,x)} \|f(y) - f(x)\|}{\min_{y\in\mathbb{S}(r,x)} \|f(y) - f(x)\|} \right). \tag{27}$$

  If f is smooth in the neighborhood of x, then H can be expressed in terms of the singular values of the Jacobian as

$$H(x, f) = \frac{\sigma_1(df_x)}{\sigma_n(df_x)}. \tag{28}$$

  Note that, clearly, $H(x, f) = K(x, f)$ for $n = 2$. Moreover, there is a direct correspondence between the facts and notations introduced in Section 2 and those for the general, n-dimensional case. Namely, let us denote by $\sigma_1(df_x) \geq \sigma_2(df_x) \geq \cdots \geq \sigma_n(df_x)$ the singular values of df_x. hen $\|df_x\| = \sigma_1$ and $l(df_x) = \sigma_n(df_x)$. (In particular, Eq. (4) can be written in the form employed in (28) above.) Moreover, since $|detdf_x|$ is the product of the singular values $\sigma_1(df_x) \geq \sigma_2(df_x) \geq \cdots \geq \sigma_n(df_x)$ of df_x, on can also express the outer and inner dilatations in terms of these singular values, as follows:

$$K_O(x, f) = \frac{\sigma_1(df_x)^{n-1}(df_x)}{\sigma_2(df_x)\cdots\sigma_n(df_x)}, \quad K_O(x, f) = \frac{\sigma_1(df_x)\cdots\sigma_{n-1}(df_x)}{\sigma_1(df_x)^{n-1}(df_x)}. \tag{29}$$

  (For more details regarding the connections between the algebraic study of df_x via its singular values and the geometric behavior at f at x see [11], Section 14, as well as [28].)

- *The isometric distortion*

$$C(f, x) = \max\{\sigma_1, \sigma_n^{-1}\} \tag{30}$$

We have the following inequalities relating between the dilatation K, the linear dilatation H and the (local) isometric distortion C:

$$K(x,f) \leq H^{n-1}(x,f) \leq C^{2(n-1)}(f,x)\,. \tag{31}$$

Note that for the aforementioned Lipschitz maps, the distortion is global (and equal to the Lipschitz constant L), and we have

$$K(f) \leq L(f)^{2(n-1)}\,. \tag{32}$$

To these one we can add

- *The local volume distortion*

$$V(f,x) = \max\left\{\sigma_1\cdots\sigma_n,\ \frac{1}{\sigma_1\cdots\sigma_n}\right\} \tag{33}$$

The following distortions measures have been proposed in the Imaging and Graphics literature

- *The Condition number*, or *aspect-ratio distortion*
  This represents nothing else than the names under which the linear distortion (in its version for smooth functions) was recently introduced, for dimensions $n = 2, 3$, in the Graphics and Imaging literature [7,8,29].

$$\kappa(f,x) = \left(\frac{\sigma_1}{\sigma_n}\right)\,.$$

- *The n-D conformal distortion*
  This distortion measure was proposed in [9]. This quantity is the ratio between the arithmetic and geometric means of the squares of singular values, namely

$$W(f,x) = \frac{1}{n}\frac{\sigma_1^2+\cdots+\sigma_n^2}{\left(\sigma_1^2\cdots\sigma_n^2\right)^{1/n}}\,; \tag{34}$$

  % where $\sigma_1^2\cdots\sigma_n^2$ denote here the eigenvalues of $df_x df_x^T$.
- *The two measures introduced in* [30]
  These can be rewritten in terms of the singular values of the Jacobian as

$$\mu(f,x) = \frac{1}{2}\left(\frac{\sigma_1\cdots\sigma_n}{v} + \frac{v}{\sigma_1\cdots\sigma_n}\right)\,; \tag{35}$$

  for a constant $v > 0$ and as a parametric distortion measure

$$\theta\mu(f,x) + (1-\theta)\frac{1}{W^{2/n}(f,x)}, \tag{36}$$

  where $1 < \theta < 0$. The last quantity can be interpreted as a convex combination of certain estimates of the conformal and the volume distortions.

References

[1] J. Ashburner, K.J. Friston, Voxel-based morphometry–the methods, Neuroimage 11 (2000) 805–821.
[2] S.S. Keller, N. Roberts, Voxel-based morphometry of temporal lobe epilepsy: An introduction and review of the literature, Epilepsia 49 (5) (2008) 741–757.
[3] Y. Zeng, C. Wang, Y. Wang, X. Gu, D. Samaras, N. Paragios, Dense non-rigid surface registration using high-order graph matching, in: Proceedings of Computer Vision and Pattern Recognition, 2010.
[4] L.M. Lui, S. Thiruvenkadam, Y. Wang, P.M. Thompson, Optimized conformal surface registration with shape-based landmark matching, SIAM J. Imag. Sci. 3 (1) (2010) 52–78.
[5] P. Caraman, n-dimensional Quasiconformal (QCF) Mappings. Revised, Enlarged and Translated from the Roumanian by the Author, Editura Academiei Române, Bucharest, Abacus Press, Tunbridge Wells Haessner Publishing, Inc., Newfoundland, NJ, 1974.
[6] Y. Wang, X. Gu, S.-T. Yau, et al., Volumetric harmonic map, in: Communications in Information & Systems, Vol. 3, International Press of Boston, 2003, pp. 191–202 3.
[7] N. Aigerman, Y. Lipman, Injective and bounded distortion mappings in 3D, ACM Trans. Graph. 32 (4) (2013) 106:1–106:14 URL http://doi.acm.org/10.1145/2461912.2461931.
[8] S.Z. Kovalsky, N. Aigerman, R. Basri, Y. Lipman, Controlling singular values with semidefinite programming, ACM Trans. Graph. 33 (4) (2014) 68.
[9] Y.T. Lee, K.C. Lam, L.M. Lui, Landmark-matching transformation with large deformation via n-dimensional quasi-conformal maps, J. Sci. Comput. 67 (2016) 926.
[10] G.-P. Paillé, P. Poulin, As-conformal-as-possible discrete volumetric mapping, Comput. Graph. 36 (5) (2012) 427–433.
[11] J. Väisälä, in: A.H. Dold, B. Eckmann (Eds.), Lectures on n-Dimensional Quasiconformal Mappings, Springer-Verlag Berlin Heidelberg New York, 1971.
[12] A. Naitsat, E. Saucan, Y.Y. Zeevi, Volumetric quasi-conformal mappings - quasi-conformal mappings for volume deformation with applications to geometric modeling, in: Proceedings of VISIGRAPP 2015, 2015, pp. 46–57, http://dx.doi.org/10.5220/0005298900460057.

[13] A. Naitsat, E. Saucan, Y.Y. Zeevi, Geometric approach to estimation of volumetric distortions, in: Proceedings of VISIGRAPP 2016, 2016.
[14] S. Rickman, Quasiregular Mappings, Springer-Verlag, Berlin, 1993, p. 15 (Chapter 1).
[15] W. Kühnel, H.-B. Rademacher, Liouville's theorem in conformal geometry, J. Math. Pures Appl. 88 (3) (2007) 251–260.
[16] T.W. Wong, W. Zeng, X. Gu, P.M. Thompson, T.F. Chan, S.-T Yau, Optimization of surface registrations using beltrami holomorphic flow, J. Sci. Comput. 50 (3) (2012) 557–585.
[17] X. Ng, T.C. Gu, L.M. Lui, Teichmuller extremal map of multiply-connected domains using Beltrami holomorphic flow, J. Sci. Comput. 60 (2) (2013) 249–275. http://dx.doi.org/10.1007/s10915-013-9791-z.
[18] L.M. Lui, K.C. Lam, S.-T. Yau, X. Gu, Teichmuller mapping (T-Map) and its applications to landmark matching registration, SIAM J. Imaging Sci. 7 (1) (2014) 391–426.
[19] W. Thurston, The Geometry and Topology of 3-Manifolds, Princeton Univ. Press, Princeton, NJ, 1990 Preliminary version edition.
[20] B.N. Apanasov, Discrete groups in space and uniformization problems, Kluwer, Dodrecht, 1992.
[21] L.V. Ahlfors, Lectures on Quasiconformal Mappings, second ed., American Mathematical Society (AMS), Providence, RI, 2006.
[22] R. Kimmel, J.A. Sethian, Computing geodesic paths on manifolds, Proc. Natl. Acad. Sci. 95 (15) (1998) 8431–8435.
[23] W.S. Torgerson, Multidimensional scaling: I. Theory and method, Psychometrika 17 (4) (1952) 401–419.
[24] S. Alhusaini, C.P. Doherty, L. Palaniyappan, C. Scanlon, S. Maguire, P. Brennan, N. Delanty, M. Fitzsimons, G.L. Cavalleri, Asymmetric cortical surface area and morphology changes in mesial temporal lobe epilepsy with hippocampal sclerosis, Epilepsia 53 (6) (2012) 995–1003.
[25] S.S. Keller, M. Wilke, U.C. Wieshmann, V.A. Sluming, N. Roberts, Comparison of standard and optimized voxel-based morphometry for analysis of brain changes associated with temporal lobe epilepsy, Neuroimage 23 (3) (2004) 860–868.
[26] L. Marsh, M.J. Morrell, P.K. Shear, E.V. Sullivan, H. Freeman, A. Marie, K.O. Lim, A. Pfefferbaum, Cortical and hippocampal volume deficits in temporal lobe epilepsy, Epilepsia 38 (5) (1997) 576–587.
[27] O. Martio, V. Ryazanov, U. Srebro, E. Yakubov, Moduli in Modern Mapping Theory, Springer, 2009.
[28] Y.G. Reshetnyak, Space Mappings with Bounded Distortion, American Mathematical Society, Providence, RI, 1989, p. 362 Ch. Translations of Mathematical Monographs 73.
[29] Y. Lipman, V.G. Kim, T.A. Funkhouser, Simple formulas for quasiconformal plane deformations, ACM Trans. Graph. 31 (5) (2012) 124:1–124:13. http://dx.doi.org/10.1145/2231816.2231822. URL http://doi.acm.org/10.1145/2231816.2231822.
[30] L. Branets, V. Garanzha, Distortion measure of trilinear mapping. Application to 3-D grid generation, Numer. Linear Algebra Appl. 9 (6–7) (2002) 511–526.